Periodic magnetospheric substorms: Multiple space-based and ground-based instrumental observations

Chao-Song Huang,[1] J. C. Foster,[1] G. D. Reeves,[2] G. Le,[3] H. U. Frey,[4] C. J. Pollock,[5] and J.-M. Jahn[5]

Received 16 April 2003; revised 25 August 2003; accepted 10 September 2003; published 25 November 2003.

[1] Quasi-periodic, sawtooth-like variations of energetic plasma particle fluxes are often measured at geosynchronous orbit during magnetic storms. The outstanding problems are whether the sawtooth flux variations represent particle injections from the tail to the inner magnetosphere, whether the sawtooth variations correspond to substorm onsets, and what mechanism is responsible for the generation of periodic particle injections (or periodic substorms). In this paper, we present the measurements of multiple space-based and ground-based instruments in the magnetosphere and ionosphere during two magnetic storms. The Geotail satellite was located in the near tail between $X_{GSM} = -20$ and -30 R_E and detected periodic southward turnings of the magnetospheric magnetic field. The southward turnings of B_z are interpreted as the signature of periodic near-tail reconnection and plasmoid formations. Geosynchronous satellites measured periodic gradual dropouts and rapid increases of energetic charged fluxes and magnetic field dipolarization. The IMAGE satellite measured enhanced emissions of energetic neutral atoms in the ring current and auroral brightenings. The Canadian Auroral Network for the OPEN Program Unified Study's photometers measured intensifications and latitudinal motion of auroral emissions. The auroral electrojet index showed periodic increases. These magnetospheric and ionospheric phenomena have the same periodicity and indicate the occurrence of periodic substorms. There is an excellent correspondence among the substorm signatures from all the measurements. The results show that periodic magnetospheric substorms can indeed occur during continuous southward interplanetary magnetic field, and the mean period in these two cases is ~2.7 hours. The sawtooth variations of energetic plasma fluxes at geosynchronous orbit represent true particle injections from the tail to the inner magnetosphere. The sawtooth injections are related to the near-tail reconnection and correspond to the onsets of periodic substorms. *INDEX TERMS:* 2788 Magnetospheric Physics: Storms and substorms; 2744 Magnetospheric Physics: Magnetotail; 2784 Magnetospheric Physics: Solar wind/magnetosphere interactions; 2730 Magnetospheric Physics: Magnetosphere—inner; *KEYWORDS:* storm, substorm, periodic substorms, sawtooth injections

Citation: Huang, C.-S., J. C. Foster, G. D. Reeves, G. Le, H. U. Frey, C. J. Pollock, and J.-M. Jahn, Periodic magnetospheric substorms: Multiple space-based and ground-based instrumental observations, *J. Geophys. Res.*, *108*(A11), 1411, doi:10.1029/2003JA009992, 2003.

1. Introduction

[2] A very interesting problem in magnetospheric substorms is whether substorms may be periodic. Geosynchronous satellites often detect a specific type of recurrent enhancements of energetic plasma particle fluxes during magnetic storms [*Borovsky et al.*, 1993; *Belian et al.*, 1995]. The recurrent variations of the fluxes can last for five to eight cycles, and the periods of the flux variations are 2–3 hours. The fluxes of energetic particles exhibit a well-defined ''sawtooth'' profile, with gradual decreases followed by rapid increases. Very similar variations of electron and proton fluxes are detected nearly simultaneously over a large local time range on the nightside. *Reeves et al.* [2003] have conducted a detailed analysis of sawtooth flux variations during the October 2000 storm. They show that the variations of geosynchronous plasma particle fluxes are closely related to the emissions of energetic neutral atoms (ENAs) in the inner magnetosphere. The ENA emissions

[1]Haystack Observatory, Massachusetts Institute of Technology, Westford, Massachusetts, USA.
[2]Los Alamos National Laboratory, Los Alamos, New Mexico, USA.
[3]Laboratory for Extraterrestrial Physics, NASA Goddard Space Flight Center, Greenbelt, Maryland, USA.
[4]Space Science Laboratory, University of California, Berkeley, Berkeley, California, USA.
[5]Department of Space Science, Southwest Research Institute, San Antonio, Texas, USA.

0148-0227/03/2003JA009992

intensify significantly when a sudden increase of plasma particle fluxes is measured, indicating that plasma particles are indeed injected to the inner magnetosphere in association with the flux increase. In addition, the sawtooth flux variations are accompanied also by magnetospheric magnetic field dipolarization and by auroral substorm signatures. The sawtooth variations of the fluxes are interpreted as the signature of periodic substorms. The flux dropout is related to the growth phase of a substorm during which the magnetospheric magnetic field is highly stretched, and the flux increase represents particle injections from the tail to geosynchronous orbit as the field undergoes dipolarization.

[3] *Huang et al.* [2003] have studied the relationship between the geosynchronous sawtooth injections and solar wind variations. They find that the sawtooth injections can be triggered by solar wind pressure impulses or modulated by solar wind pressure oscillations. For continuous solar wind pressure oscillations, there is a correspondence between each cycle of the solar wind pressure oscillations and each cycle of the sawtooth injections. For isolated solar wind pressure impulses, the sawtooth injections occur after the solar wind pressure impulses impinge on the magnetosphere. Sawtooth injections can continue for several cycles after being triggered, even though the solar wind has become stable, implying that the period of the sawtooth injections is determined by the magnetosphere. The sawtooth injections occur during the main phase and/or initial recovery phase of magnetic storms. They suggest that magnetospheric substorms have an intrinsic cycle time of 2–3 hours. If solar wind pressure oscillations with periods comparable to the substorm cycle time are imposed on the magnetosphere, some magnetospheric resonant state may be excited, and periodic substorms will occur. The magnetosphere is highly dynamic during magnetic storms, so the resonance can be excited more easily. Otherwise, if the solar wind oscillates too fast, enough energy is not accumulated in the magnetotail for substorms to occur; if the period of solar wind pressure oscillations is too long, magnetospheric energy may be released through other processes, including internally triggered substorms.

[4] On the other hand, dropouts of energetic particle fluxes may be also detected by a geosynchronous satellite when the satellite enters the lobe [*Thomsen et al.*, 1994; *Moldwin et al.*, 1995]. Lobe encounters at geosynchronous orbit are generally associated with large geomagnetic storms and large solar wind disturbances that are characterized by strongly southward interplanetary magnetic field (IMF) and enhanced solar wind dynamic pressure. Under such solar wind and geomagnetic conditions, the magnetosphere can be highly distorted, and the lobes may move to geosynchronous orbit. A geosynchronous satellite will detect a dropout of plasma particle fluxes when it moves from the plasma sheet to the lobes and a flux enhancement when it moves from the lobe to the plasma sheet.

[5] There are some similarities in the appearance of the flux variations between the lobe encounters and sawtooth variations. The sawtooth flux variations are observed during magnetic storms and continuously southward IMF after solar wind pressure impulses/oscillations impinge on the magnetosphere [*Huang et al.*, 2003]. The magnetosphere is highly dynamic during magnetic storms, and solar wind pressure oscillations and impulses can cause significant disturbances in the magnetosphere. The question is whether the sawtooth flux variations represent substorm injections or are caused by large disturbances in a highly distorted magnetosphere.

[6] In order to verify that the sawtooth flux variations indeed correspond to substorms, the following questions must be answered. (1) Could the observed sawtooth mechanisms generate periodic substorms? (2) Does the signature of the newly injected particles in the inner magnetosphere, in the case of sawtooth flux variations, correspond to that for substorms? (3) Are sawtooth flux variations associated with substorm-like auroral displays?

[7] We will present observations of multiple space-based and ground-based instruments during two magnetic storms. A unique characteristic of the observations is that the Geotail satellite was located in the near tail between $X_{GSM} = -20$ and -30 R_E and detected periodic (2–3 hours) magnetic reconnection and plasmoid formations. Other satellites detected sawtooth flux variations at geosynchronous orbit, energetic neutral atom emissions in the ring current, and auroral brightenings. Ground photometers and magnetometers detected auroral intensifications. All measurements show a very good temporal correlation. The purpose of this paper is to provide a complete picture of periodic substorms from the generation mechanism to processes in the inner magnetosphere and to auroral signatures and thereby demonstrate the plausibility of the hypothesis that sawtooth flux variations observed at geosynchronous orbit are actually due to periodic magnetospheric substorm activity.

2. Observations

[8] We first present the observations on 18 April 2002. The Geotail satellite was located in the northern lobe between $X_{GSM} = -21$ and -29 R_E on this day. Shown in Figure 1 are the magnitude and the three components of the magnetospheric magnetic field with 3-s time resolution measured by Geotail; the Geotail position is given in the bottom of Figure 1. The most prominent feature in Figure 1 is the periodic oscillations in the field strength and all three components. Seven cycles of oscillations occurred between 0000 and 1900 UT, with a mean period of ~2.7 hours. The vertical dotted lines are used to indicate the peaks of the field strength and southward turnings of the magnetic field **B** (B_z became negative) at 0036, 0241, 0530, 0812, 1142, 1413, and 1634 UT. The magnetospheric oscillations continued for several cycles after 1800 UT, while B_z showed decreases but did not become negative.

[9] The magnetic field B_z component in the lobes is generally positive. The southward turnings of B_z may be related to the formation of plasmoids. Plasmoids are initially formed at the near-Earth neutral line between $X_{GSM} = -20$ R_E and -30 R_E, and the magnetic signature of the passage of a plasmoid through an observer (satellite) in the plasma sheet is characterized by a northward and then southward deflection of the magnetic field B_z component [*Hones et al.*, 1984; *Baker et al.*, 1987; *Moldwin and Hughes*, 1992; *Nagai et al.*, 1998a, 1998b; *Ieda et al.*, 1998]. Plasmoids can also be "remotely" sensed in the tail lobes [*Slavin et al.*, 1984, 1993; *Taguchi et al.*, 1998]. When a plasmoid moves tailward

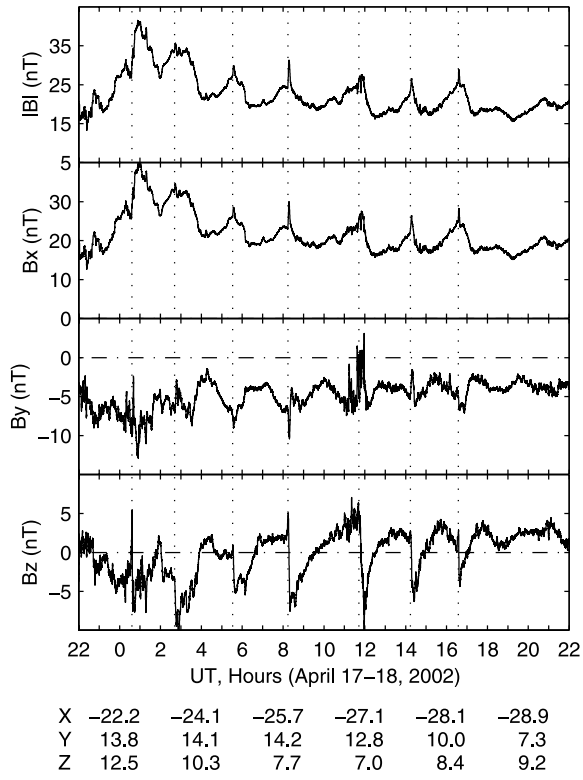

Figure 1. The magnitude and components of the magnetospheric magnetic field measured by the Geotail spacecraft between 2200 UT on 17 April and 2200 UT on 18 April 2002. The magnetic field components and Geotail position at the bottom of the figure are given in geocentric solar magnetospheric (GSM) coordinates. The vertical dotted lines indicate the peaks of the field strength and southward turnings of the B_z component.

in the center of the magnetotail, the plasmoid causes a bulge in the plasma sheet which compresses the lobe field against the magnetosheath. As the bulge passes, lobe field line tilting causes an increase in the lobe field magnitude and a north-to-south deflection of the B_z component. This lobe signature of plasmoids is termed the traveling compression region.

[10] *Huang* [2002] has made a detailed analysis of the Geotail magnetic and plasma particle data on 18 April 2002. The magnetic field B_z component showed a northward increase before it turned southward. He suggests that the southward turnings of B_z represent magnetic reconnection onsets in the near tail and that the enhancements of the magnetic field strength represent the compressions of the lobe field by tailward moving plasmoids. Geotail must be located tailward of the center of the plasmoid in order to detect a northward increase of B_z. When the plasmoid center moved to Geotail, the field compression reached a maximum value, and B_z became zero. Then B_z became negative when Geotail was earthward of the plasmoid center. This is exactly what has been observed. The variation of the magnetic field can be divided into three distinct intervals during each cycle. The first interval is characterized by a rapid increase of the field strength during the growth phase of substorms, the second interval is characterized by negative B_z during the expansion phase, and the third interval is characterized by a slow increase or a largely unchanged field during the recovery phase. The average time of the expansion phase is 63 min, and both the growth and recovery phases take ~40 min. In the following, we will use magnetic reconnection onsets and plasmoid formations to interpret the near-tail magnetic variations shown in Figure 1; the vertical dotted lines indicate the reconnection onsets.

[11] We now take a look at the energetic plasma particle fluxes at geosynchronous orbit. Figure 2 shows the electron and proton fluxes measured by the LANL satellites 1990–095 (magnetic local time (MLT) = UT − 2.5 hours) and 1991–080 (MLT = UT − 8 hours); no proton data are available from 1990–095. The vertical dotted lines in Figure 2 indicate the southward turnings of the Geotail magnetic field B_z (reconnection onsets) identified from Figure 1. A salient feature in Figure 2 is the excellent coincidence between the reconnection onsets in the near tail and the energetic flux increases at geosynchronous orbit, and a one-to-one correspondence exists clearly. The flux increases are almost simultaneous in all energy channels, without noticeable time delay. We use the term "injections" to describe the flux increases and will show that this is true below. Such simultaneous flux increases represent dispersionless injections, and particles in the whole energy range are injected nearly simultaneously into the satellite position. After being injected into the inner magnetosphere, electrons are driven by the magnetic gradient/curvature to drift eastward. If a satellite is located westward of the injection region, it will see an energy dispersion. The flux increases in the 1990–095 measurements were nearly dispersionless between 0000 and 0600 UT and became dispersive after 0600 UT. This means that 1990–095 was within the injection region between 0000 and 0600 UT and was eastward of the injection region after 0600 UT. In contrast, the 1991–080 data showed small variations in the electron fluxes and large variations in the proton fluxes before 0600 UT. At 0530 UT, 1991–080 was at ~2130 MLT; the large increases of proton fluxes and small variations of electron fluxes imply that 1991–080 was westward of the injection region. The measurements of the two satellites make it possible to determine the injection region which was between 2130 and 0300 MLT in the midnight sector. *Reeves et al.* [1990, 1992] studied the injection region of energetic particles in association with an isolated substorm and found that the injection region spanned ~90° in local time around midnight. The sawtooth injections in the present case occurred in the same region as the isolated substorm injections.

[12] An important phenomenon associated with substorm onsets is the dipolarization of the magnetic field in the inner magnetosphere [*Baumjohann et al.*, 1999]. The magnetospheric magnetic field is highly stretched during the growth phase of substorms and suddenly becomes more dipolar in the inner magnetosphere after the substorm onsets. The dipolarization may be related to cross-field current instability and current disruption [*Lui*, 1991, 1996; *Ohtani et al.*, 1992], plasma interchange instability [*Roux et al.*, 1991], drift ballooning instability [*Pu et al.*, 1999], and near-tail reconnection and plasmoid formation [*Fairfield et al.*, 1998]. The dipolarization is the signature of a dramatic reconfiguration of the magneto-

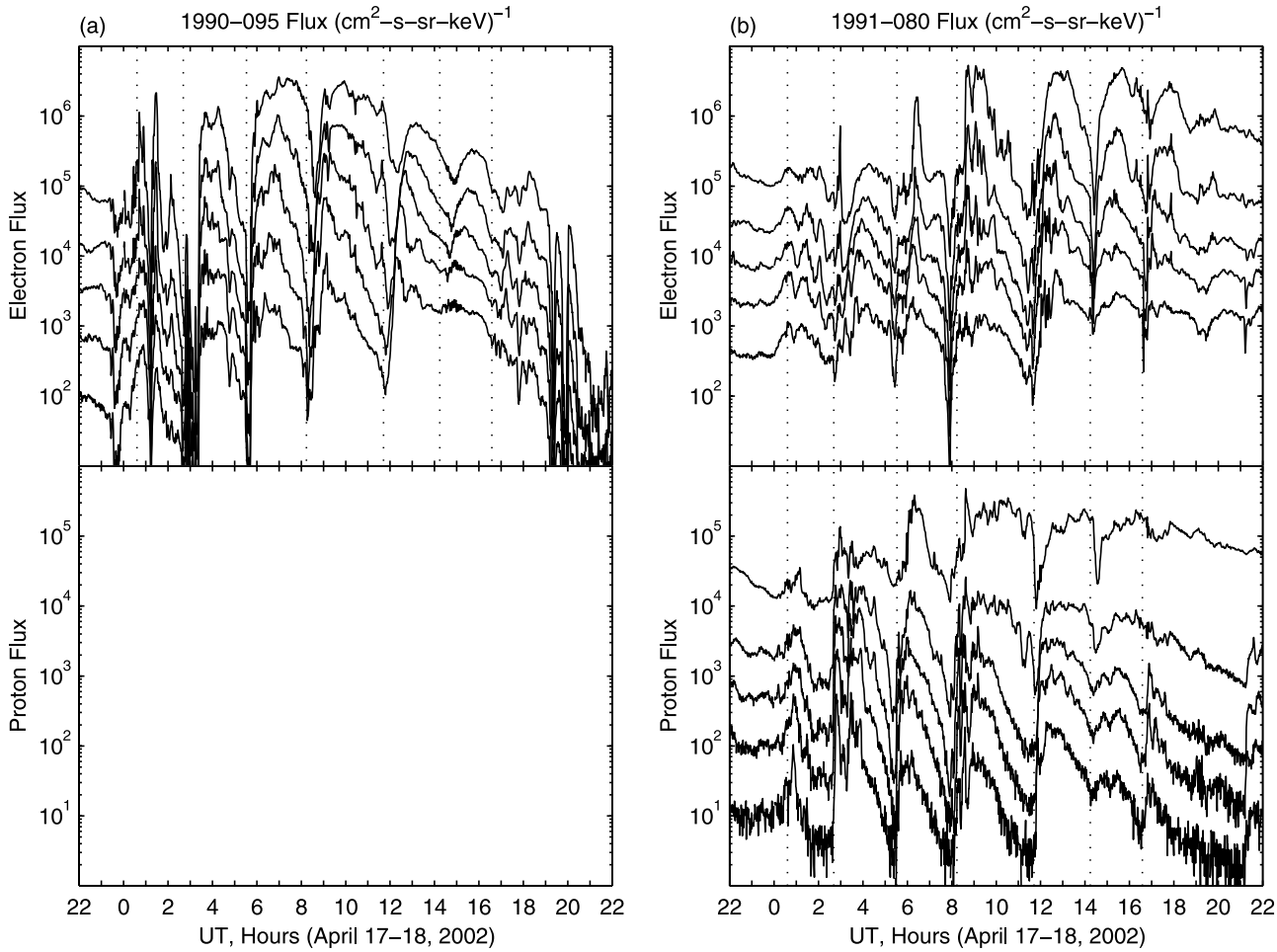

Figure 2. Electron and proton fluxes measured by the geosynchronous satellites LANL 1990–095 and 1991–080 between 2200 UT on 17 April and 2200 UT on 18 April 2002. The electron energy channels are 50–75, 75–105, 105–150, 150–225, and 225–315 keV. The proton energy channels are 50–75, 75–113, 113–170, 170–250, and 250–400 keV. The vertical dotted lines indicate the times of the southward turnings of the magnetic field B_z component measured by Geotail, identified from Figure 1.

sphere during substorms and is characterized by the magnetic field elevation in the plasma sheet. The elevation angle is the angle between the magnetic field direction and the equatorial plane and is defined as $\tan^{-1}(B_z/(B_x^2 + B_y^2)^{1/2})$. Figure 3 shows the elevation angle measured by the geosynchronous satellites GOES 8 (MLT = UT − 5 hours) and GOES 10 (MLT = UT − 9 hours). The vertical dotted lines indicate the times of the near-tail reconnection onsets. The dipolarization was measured in association with the first five onsets. The dipolarization at 0812 and 1142 UT was large at the GOES 10 position (2312 and 0242 MLT) and small at the GOES 8 position (0312 and 0642 MLT), and no clear dipolarization signature was registered by GOES 10 at 1413 and 1634 UT (0513 and 0734 MLT), although the reconnection onsets were measured by Geotail in the tail. This implies that the dipolarization is large in the midnight sector between 2100 and 0300 MLT, consistent with the region of energetic particle injections. The dipolarization in the inner magnetosphere results from magnetic compressions from earthward plasma flow. When the satellites are within the region of the earthward flow, they are capable of detecting the dipolarization.

[13] When energetic plasma particles are injected to the inner magnetosphere, the charged particles collide with neutral atoms and become neutrally charged. Enhanced emissions from the newly produced ENAs are a consequence of substorm injections [e.g., *Reeves and Henderson*, 2001; *Reeves et al.*, 2003]. The Imager for Magnetopause-to-Aurora Global Exploration (IMAGE) satellite [*Burch et al.*, 2001] has extensive instrumentations for detecting and making images of energetic neutral particle emissions from the inner magnetosphere. The medium-energy neutral atom (MENA) imager detects ENAs in the energy range 1–30 keV. Shown in Figure 4 are the images from the MENA imager at 0520–0529, 0551–0600, 0620–2629, and 0650–0659 UT on 18 April 2002. Each image is integrated over 9 min. The color scale is logarithmic and the same for all images. The white curves represent dipole field lines at $L = 4$ and 8. Local noon is near the bottom of each image and is indicated in red, and local dusk is to the right of each image. The ENA emissions were rather weak before 0540 UT and significantly intensified after 0540 UT.

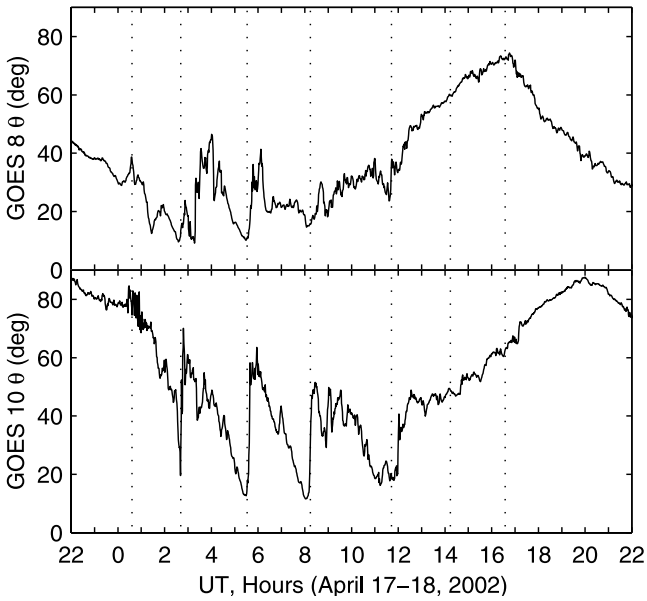

Figure 3. Magnetospheric magnetic field elevation angle measured by the geosynchronous satellites GOES 8 and GOES 10. The vertical dotted lines indicate the times of the southward turnings of the magnetic field B_z component measured by Geotail.

Figure 2 shows that there was a sudden increase in the energetic plasma flux at 0530 UT. The intensified ENA emissions in the inner magnetosphere occurred exactly after the increase of the plasma particle fluxes at geosynchronous orbit, providing unambiguous evidence that the plasma flux increase detected by geosynchronous satellites was a true injection and that the injected particles caused the enhanced ENA emissions. The measurements of the ENA emissions depend on the position of the detector (the satellite), so the MENA (and other ENA) instruments may not be able to detect periodic enhancements of the emissions over a long interval of many hours. Because all flux increases of the sawtooth variations have the same characteristics, it is reasonable to conclude that each flux increase can be interpreted as one injection and that the sawtooth flux variations represent periodic injections.

[14] As discussed in section 1, one of the fundamental features of substorms is the auroral brightening that is caused by particle precipitation from the magnetosphere to the ionosphere during substorms [*Akasofu*, 1968]. We present in Figure 5 the auroral images obtained by the Far Ultra-Violet Wideband Imaging Camera (FUV/WIC) on board the IMAGE satellite between 0234 and 0638 UT on 18 April 2002. The auroral images are shown every 2 min. The orientation is such that local noon is to the left and dusk is to the bottom of each image. There was some enhanced auroral activity in the premidnight sector between 0240 and 0313 UT. A brightening became very clear near midnight at 0315 UT and then expanded in local time and latitude. A second auroral brightening started to occur near midnight at 0530 UT. Although not shown here, there was a third brightening starting at 0812 UT. The Geotail measurements (Figure 1) show that southward turnings of B_z occurred at 0241, 0530, and 0812 UT. Corresponding to the B_z southward turning measured by Geotail at 0241 UT, the geosynchronous flux data (Figure 2) show that a short-lived injection occurred at 0241 UT and a much stronger injection occurred at 0323 UT. It appears that there were some complex processes active in the magnetosphere during this interval. As a result, the auroral brightening also showed some complex behavior. The auroral brightenings at 0530 and 0812 UT, as well as the brightening at 0315 UT, coincided very well with the corresponding reconnection onsets and energetic particle injections. The excellent coincidence between the geosynchronous injections and auroral brightenings provides a clear evidence that the particle injections correspond to substorm onsets.

[15] The auroral brightenings can be also monitored by ground-based measurements. Figure 6 shows the optical data obtained by the Canadian Auroral Network for the OPEN Program Unified Study (CANOPUS) meridian scanning photometers [*Rostoker et al.*, 1995]. The plots show the emission intensities as a function of invariant latitude and UT. The 557.7-nm emissions result from the precipitation of >1 keV electrons, the 486.1-nm emissions result from proton precipitation, and the 630.0-nm emissions result from the precipitation of <1 keV electrons and also respond to proton precipitation. The auroral intensifications are a typical signature of substorm onsets.

[16] The photometers were in an excellent location for monitoring nightside auroral activity during the period of interest. There are several important features in the optical data of Figure 6. (1) All 557.7-, 486.1-, and 630.0-nm emissions intensified greatly at ~0240 and ~0530 UT, indicating enhanced precipitation of both electrons and protons. Another intensification, although it is not so clear as the first two, occurred in the Fort Smith photometer data at ~0812 UT. (2) The intensifications occurred exactly at the same time as the reconnection onsets in the near tail and the energetic particle injections at geosynchronous orbit. As can be seen from Figures 1 and 2, the corresponding near-tail reconnection and geosynchronous injections were observed at 0241, 0530, and 0812 UT. (3) The auroral substorm onsets occurred at lower latitudes. The enhanced auroral emission bands moved equatorward during the growth phase of the substorms and poleward after the onsets. For example, the onset at 0530 UT from the Pinawa photometer occurred at 61°, and the auroral emission bands moved equatorward from ~66° at 0430 UT to ~61° at 0530 UT and then expanded rapidly poleward to ~68° at 0545 UT. MLT at Pinawa is about UT − 7 hours, and MLT at Fort Smith is about UT − 8.5 hours. The auroral zone is located at lowest latitudes near midnight. Pinawa was closer to midnight between 0400 and 0600 UT (between 2100 and 2300 MLT) and therefore detected the emission bands at lower latitudes. The important point is that these observations correspond to the classic substorm behavior, whereby the auroral intensifications start to occur at lower latitudes at the substorm onset and then move to higher latitudes during the expansion phase.

[17] The auroral activity can also be detected with ground magnetometers. Enhanced particle precipitation in the nightside auroral zone results in large enhancements of the ionospheric conductivity and currents. A major element in the current system associated with substorms is termed the "substorm current wedge" [*McPherron et al.*, 1973].

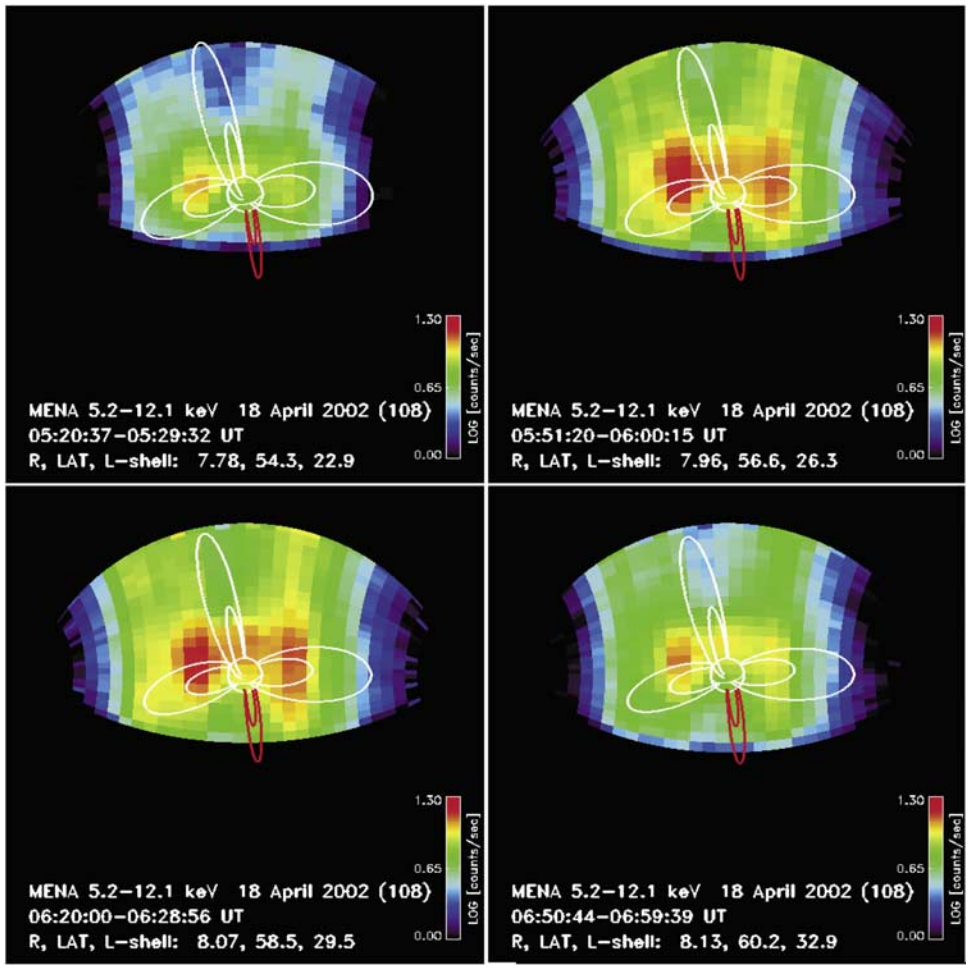

Figure 4. Energetic neutral atom images collected by the IMAGE satellite at 0520, 0551, 0620, and 0650 UT on 18 April 2002. The emission intensified after 0540 UT.

When ground magnetometers are located near the midnight sector, they can detect the auroral electrojet, which closes the ionospheric portion of the circuit connected to the substorm current wedge. Figure 7 shows the *H* (northward) component of magnetic deviations at auroral latitudes detected by the CANOPUS magnetometer array. MLT at FCHU, GILL, ISLL, and PINA is about UT − 7 hours, and MLT at DAWS is about UT − 11 hours. The magnetometers detected negative (southward) magnetic deviations after each reconnection onset. The deviations were large at FCHU, GILL, ISLL, and PINA between 0200 and 1000 UT (1900 and 0300 MLT). In contrast, large negative deviations at DAWS occurred between 0500 and 1800 UT (1800 and 0700 MLT). The negative magnetic deviations are related to westward auroral electrojet currents, indicating that the auroral current was enhanced by the substorm activity.

[18] The expansion of the auroral zone or the motion of the auroral boundary can be also seen from the magnetometer data. We present in Figure 8 the magnetic deviations in an expanded timescale. The four magnetometers are located at about the same longitude. The poleward expansion of the enhanced westward auroral electrojet is clearly shown. The magnetic deviation started at PINA at ~0530 UT, and then expanded to ISLL at 0537 UT, to GILL at 0540 UT, and to FCHU at 0545 UT, as indicated by the vertical dashed lines. The poleward expansion of the auroral electrojet is very consistent with the poleward expansion of the auroral intensification of the 630.0-nm emissions from the Pinawa photometer shown in Figure 6.

[19] We investigate the possible effect of periodic substorms on the subauroral region by exploring the characteristics of the subauroral polarization streams (SAPS). The motion of the auroral zone in response to substorms has a corresponding signature in the subauroral region. During geomagnetic disturbances, large westward plasma flow, which is separate from the conventional auroral return flow in the afternoon convection cell, often occurs at subauroral latitudes in the evening sector [*Yeh et al.*, 1991; *Huang et al.*, 2001]. The westward flow covers about ~5° in latitude, and its amplitude can be as high as 3000 m s^{-1}. This fast flow has been termed as subauroral ion drift (SAID), polarization jet (PJ), and recently as subauroral polarization streams (SAPS) [*Foster and Burke*, 2002; *Foster and Vo*, 2002]. SAPS are associated with magnetospheric-ionospheric coupling and ionospheric feedback in the region where magnetospheric field-aligned currents attempt to close across the subauroral ionosphere. Enhanced magnetospheric disturbances will cause corresponding variations in the location and amplitude of SAPS. Shown in Figure 9

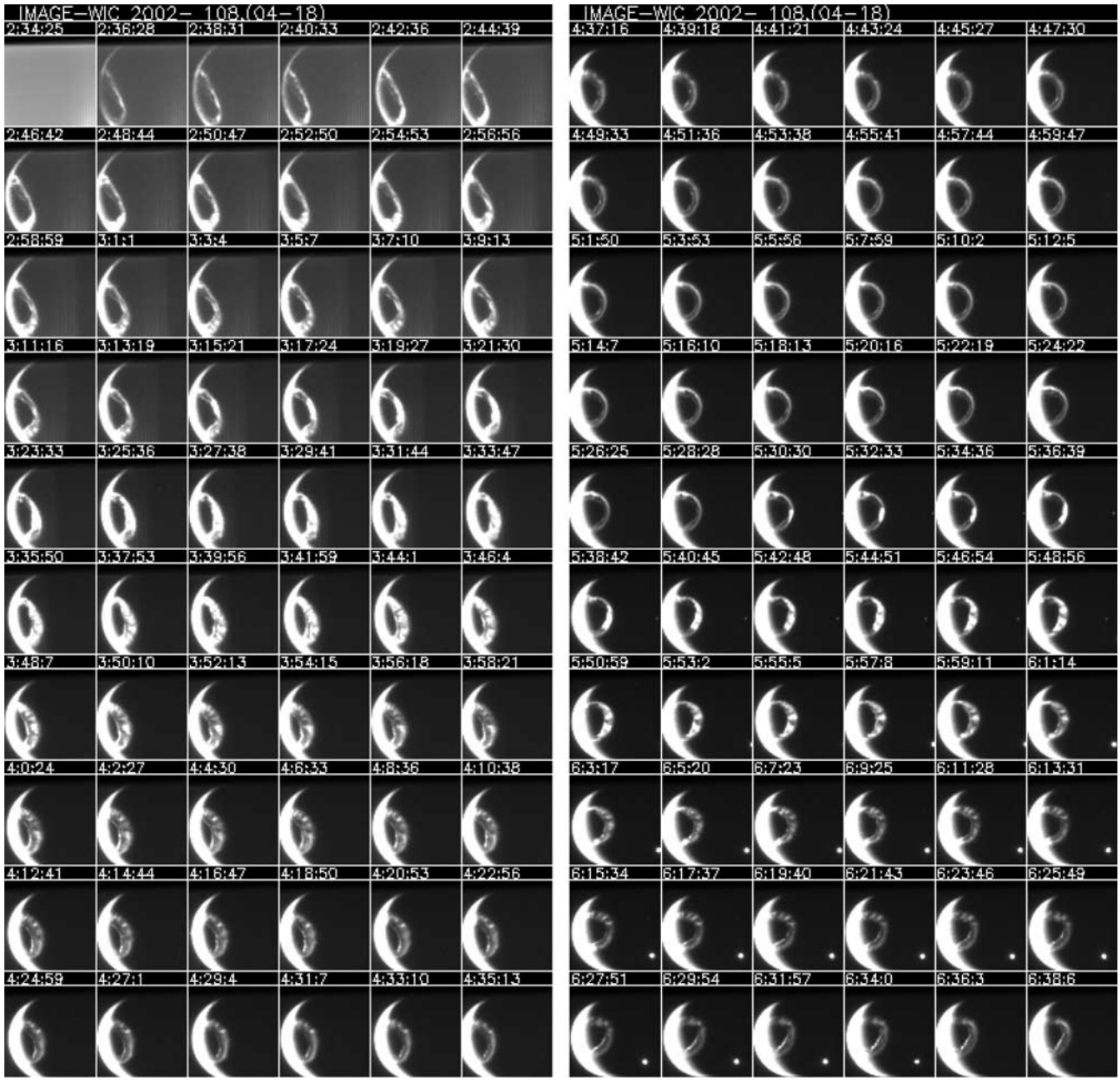

Figure 5. Auroral images measured by the FUV instrument on board the IMAGE satellite between 0234 and 0638 UT on 18 April 2002. Auroral brightenings started to occur at 0248 and 0530 UT.

are the location (geomagnetic latitude) and magnitude of the maximum velocity of the SAPS measured by the Defense Meteorological Satellite Program (DMSP) spacecrafts F13, F14, and F15 which passed the Northern Hemispheric subauroral zone at ~1800, ~2000, and ~2100 MLT, respectively. The vertical dotted lines indicate the times of the reconnection onsets identified from Figure 1. There is a general correspondence between variations in the negative latitude peaks/positive velocity peaks of the SAPS and the periodicity of the reconnection onsets. The observations of Figure 9 are suggestive of a relationship between periodic substorms and subauroral field-aligned currents and SAPS electric fields. We include this comparison here for completeness.

[20] The correspondence of the substorm onsets among different measurements has been shown by the vertical dotted lines in Figures 1–9. It is instructive to depict different measurements in one plot. We present in Figure 10 the magnetospheric magnetic field B_z component measured by Geotail in the near tail, the electron flux of 105–150 keV measured by the LANL 1990–095 satellite at geosynchronous orbit, the magnetospheric magnetic field elevation angle measured by GOES 10, the geomagnetic disturbance symmetric component SYM-H, and the CL index. The SYM-H index is equivalent to the *Dst* index and represents the variations of the ring current. The CL index is the lower envelope of the CANOPUS magnetometer *H* deviations and is a local equivalent to the auroral electrojet geomagnetic (*AL*) index. The negative deviations of CL correspond to the enhancements of the auroral electrojet during substorms. The vertical dotted lines again indicate the times of the southward turnings of the Geotail B_z. The

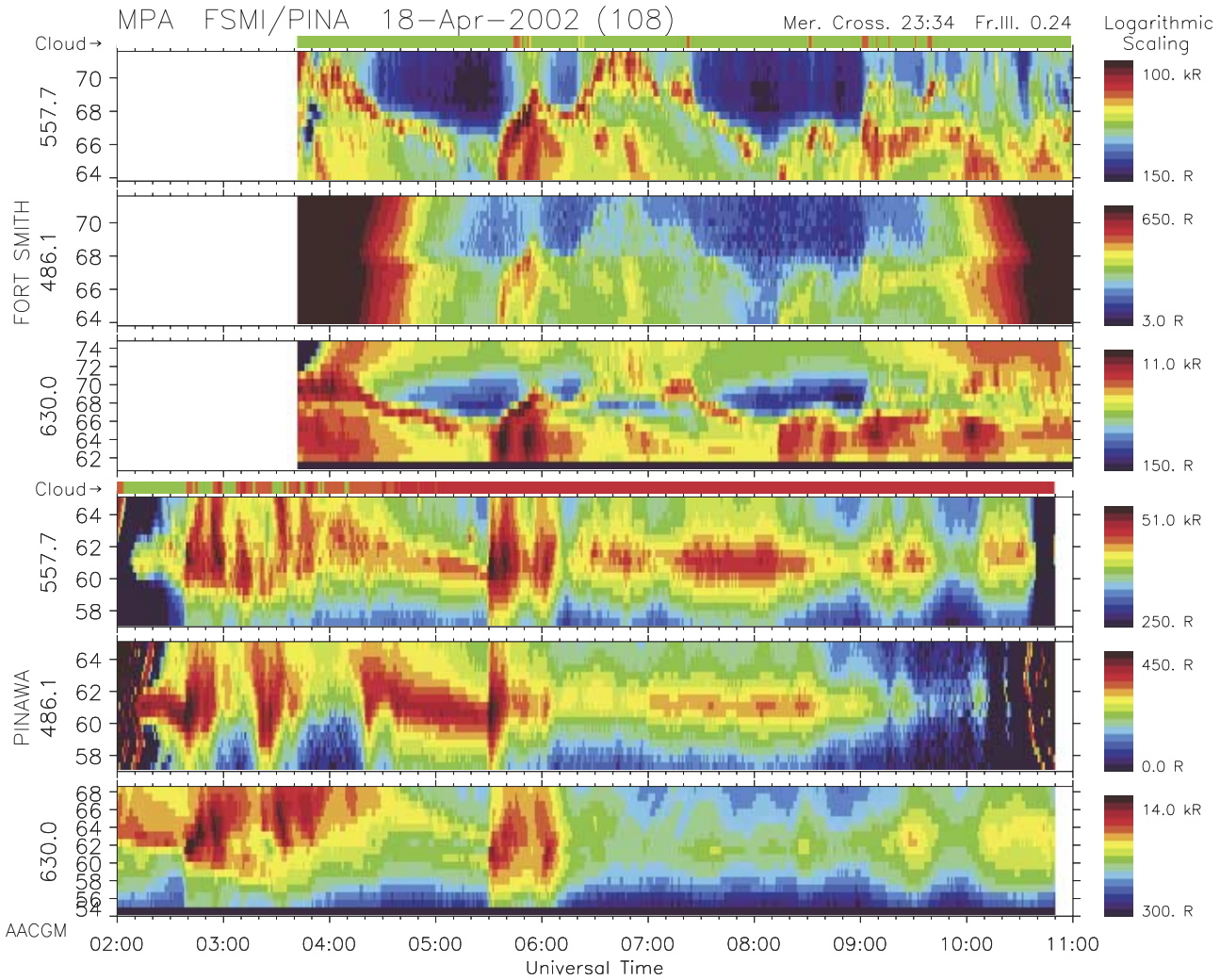

Figure 6. Auroral luminosity obtained by scans of the 557.7-, 486.1-, and 630.0-nm auroral lines from the Fort Smith and Pinawa meridian scanning photometers between 0200 and 1100 UT on 18 April 2002. Auroral intensifications occurred around 0240, 0530, and 0810 UT.

good correspondence in all measurements indicates that the periodic variations in all the magnetospheric and ionospheric parameters represent the signatures of periodic substorms.

[21] An interesting phenomenon in Figure 10 is that SYM-H shows an increase (or becomes less negative) after each onset (or each injection). In general, it is believed that the ring current is enhanced after energetic particles are injected from the tail to the inner magnetosphere, which should result in a decrease (more negative) in the *Dst* and SYM-H indices. The observed variations of SYM-H may imply that SYM-H (or *Dst*) is also effected by other magnetospheric currents beside the ring current. It has been suggested that the increase in SYM-H (or *Dst*) after substorm onsets is related to a reduction in the cross-tail current [*Iyemori and Rao*, 1996; *Siscoe and Petschek*, 1997].

[22] In order to see the precise timing of the substorm signatures, we present some measurements in Figure 11 in an expanded timescale. Two vertical dotted lines are plotted at 0530 and 0812 UT. The magnetic field strength and B_z component measured by Geotail started to increase at these times. As discussed by *Huang* [2002], Geotail was located tailward of the reconnection site. The increase in the field strength represents the formation of a plasmoid, and the maximum strength corresponds to the moment at which the plasmoid center moved across the satellite. The plasma injections show some subtle differences. The 1990–095 satellite was located in the postmidnight sector (0300 MLT) at 0530 UT and near dawn (0542 MLT) at 0812 UT. The electron flux increases (injections) measured by 1990–095 showed a sudden decrease at 0530 UT and then started to increase rapidly at 0542 UT. It is not clear what caused the sudden decrease of the electron flux at the 1990–095 position. For the reconnection onset at 0812 UT, the 1990–095 electron flux started to increase at 0821 UT, about 9 min later than the corresponding reconnection onset. Since electrons drift eastward after being injected, the delay in the 1990–095 measurements after the 0812 UT onset may represent the fact that the particles were injected westward of the satellite and took ~9 min to drift to the satellite position. The 1991–080 satellite detected a proton injection exactly at 0530 UT (~2130 MLT), the time of the corresponding reconnection onset. However,

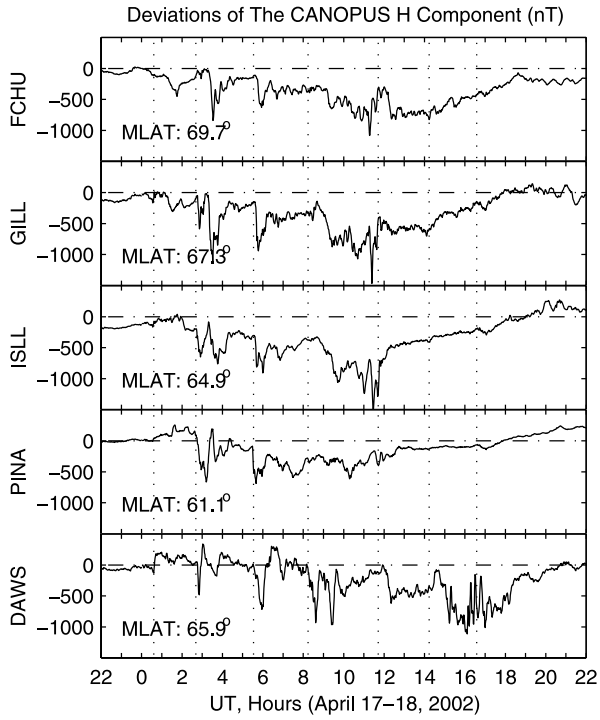

Figure 7. The northward (H) component of ground magnetic field deviations measured with the CANOPUS magnetometers. The names, abbreviations, and geographic coordinates of the stations are Fort Churchill (FCHU, 265.9°E, 58.7°N), Gillam (GILL, 265.3°E, 56.3°N), Island Lake (ISLL, 265.3°E, 53.8°N), Pinawa (PINA, 263.9°E, 50.2°N), and Dawson (DAWS, 220.8°E, 64.0°N). The geomagnetic latitude (MLAT) of each station is given in the figure. The vertical dotted lines indicate the times of the southward turnings of the magnetic field B_z component measured by Geotail.

the next proton injection was detected to start at 0755 UT (~0000 MLT), which was ~17 earlier than the reconnection onset at 0812 UT. The magnetic field dipolarization angle detected by GOES 10 and the ground magnetometer deviations measured at PINA and DAWS coincided well with the corresponding reconnection onsets. The Geotail magnetic field data have a time resolution of 3 s, and the ground magnetometer data have a time resolution of 5 s. Figure 11, as well as Figures 5, 6, and 8, shows that the auroral intensifications started almost exactly at the times when the reconnection onsets occurred in the near tail. No noticeable time delay can be identified between the near-tail reconnection onsets and auroral intensifications in the present case.

[23] The occurrence of the periodic substorms is related to a sudden change in the solar wind. Figure 12 shows, from top to bottom, the solar wind velocity, solar wind ion density, solar wind dynamic pressure, and three IMF components measured by the Wind satellite which was located at X_{GSM} = 9–12 R_E on 18 April 2002. A sudden change in all the solar wind parameters was measured by Wind at 0010 UT on 18 April, as indicated by the vertical dotted line. The solar wind velocity decreased from 602 to 530 m s^{-1}, the solar wind pressure showed a large impulse, and three IMF components showed a short-lived (~18 min) increase. The sudden change in the solar wind coincided well with the first substorm onset at 0036 UT. Perhaps, it is the solar wind pressure impulse, in combination with the spike in the IMF components, that triggered the periodic substorms. It is important to note that the solar wind was rather stable after the pressure impulse. However, the substorms continued to occur for many cycles. The IMF B_z was continuously negative during the interval of the periodic substorms.

[24] The periodic substorms occurred during a magnetic storm. We present in Figure 13 the solar wind dynamic pressure, the IMF B_z component, and the *Kp*, *Dst*, and SYM-H indices during 17–19 April 2002. SYM-H has a time resolution of 1 min, while *Dst* has a time resolution of 1 hour. A solar wind shock was measured by Wind at 1100 UT on 17 April. The solar wind pressure increased from 4 to 23 nPa across the shock, and the IMF B_z showed large fluctuations after the shock. A magnetic storm was driven by the interplanetary shock, *Dst* increased from −22 nT at 1000 UT on 17 April to 2 nT at 1100 UT and then decreased rapidly. The periodic magnetospheric substorms occurred on 18 April, indicated by the shaded interval in Figure 13, during the late stage of the main phase and first stage of the recovery phase of the storm.

[25] The second case we are going to study occurred on 18 February 1999. All major characteristics in this case are very similar to those of the first case. Here we give a brief description of the magnetic history. A solar wind pressure impulse and associated IMF southward turning caused a

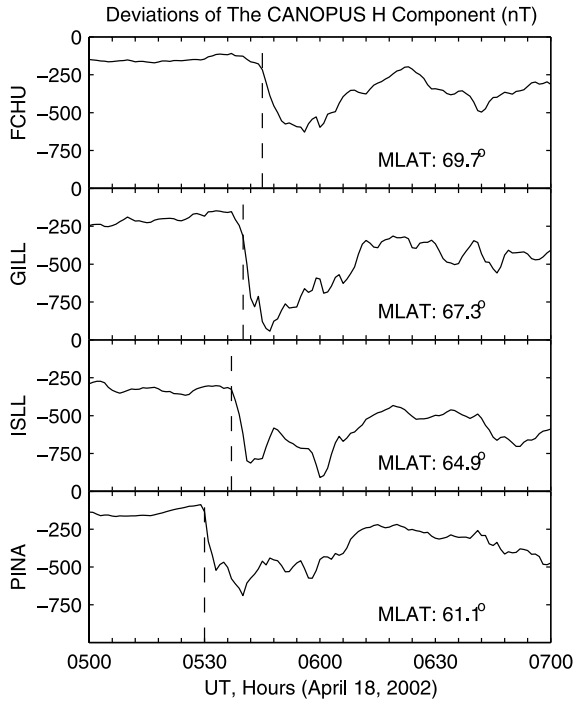

Figure 8. The northward (H) component of ground magnetic field deviations measured at FCHU, GILL, ISLL, and PINA between 0500 and 0700 UT on 18 April 2002. The negative deviations started to occur first at lower latitudes and then moved to high latitudes, as indicated by the vertical dashed line.

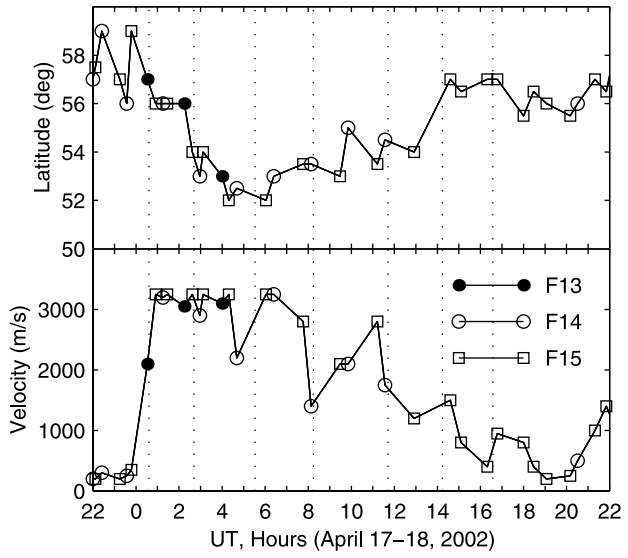

Figure 9. The latitudinal location and magnitude of the maximum velocity of subauroral polarization streams measured by the DMSP spacecrafts F13, F14, and F15. The vertical dotted lines indicate the times of the southward turnings of the magnetic field B_z component measured by Geotail.

magnetic storm at ~0300 UT on 18 February 1999. The *Dst* index decreased from 2 nT at 0300 UT to −123 nT at 0900 UT and then started to recover. The periodic magnetospheric substorms, which will be discussed below, occurred between 0250 and 2400 UT during the main phase and initial recovery stage of the storm.

[26] The solar wind velocity, ion density, and dynamic pressure, and three IMF components of this second case are shown in Figure 14. The Wind satellite was located at about $X_{GSM} = -8\ R_E$, $Y_{GSM} = -40\ R_E$, and $Z_{GSM} = -40\ R_E$ on 18 February 1999. The Y and Z coordinates suggest that Wind was in the solar wind. We checked the ACE ($X_{GSM} = 243\ R_E$) measurements on this day; the ACE data are, after a time shift, in perfect agreement with the Wind data. The most significant change in the solar wind is the pressure impulse at 0245 UT, as indicated by the vertical dotted line. The solar wind pressure jumped from 1 to 8 nPa, and all other solar wind parameters showed a sudden change. The big solar wind pressure impulse would suddenly compress the magnetosphere, resulting in significant oscillations in the magnetosphere. The expected compression and oscillations of the magnetosphere indeed occurred.

[27] Figure 15 shows the magnetospheric field and particle data measured by the Geotail satellite which was located in the central plasma sheet between $X_{GSM} = -30$ and $-21\ R_E$ on 18 February 1999. Figure 15a shows the strength and three components of the magnetospheric magnetic field with 3-s time resolution, and Figure 15b shows the ion density, ion energy, ion pressure, and ion velocity X (earthward) component with a time resolution of 1 min. At 0250 UT, the field strength was suddenly increased from 12 to 37 nT within 10 min. Obviously, this represents the compression of the magnetosphere by the solar wind pressure impulse. After the compression, quasiperiodic oscillations occurred in the magnetosphere. Eight cycles of oscillations occurred between 0200 and 2400 UT, with a mean period of ~2.75 hours. The vertical dotted lines are used to indicate the major changes in the magnetic field and particle data at 0250, 0454, 0728, 0937, 1255, 1512, 1816, 2026, and 2300 UT. The first line at 0250 UT is related to the sudden compression, and no southward turning of B_z occurred at this moment. The subsequent seven lines indicate the southward turnings of the B_z component. In general, the ion energy and pressure decreased significantly after each southward turning of B_z. The ion velocity was positive (earthward) before the B_z southward turnings and became negative (tailward) after the B_z southward turnings. The tailward velocity of the ions was 600–1000 km s^{-1} and lasted 40–60 min in association with the B_z southward turnings at 0728, 0937, and 1255 UT.

[28] The variations of the magnetic field and plasma particles are readily explained with the near-tail reconnection scenario proposed by *Huang* [2002]. Assume that Geotail was within the central plasma sheet and that the reconnection onsets occurred earthward of Geotail. Before a reconnection onset, Geotail was in the plasma sheet and measured high-energy and high-pressure plasma, and the plasma velocity in the sheet was earthward. After a reconnection onset, a plasmoid formed and moved tailward across Geotail. Therefore Geotail measured southward magnetic field and negative (tailward) ion velocity associated with the plasmoid. After the plasmoid passed the satellite, the satellite detected plasma particles that were

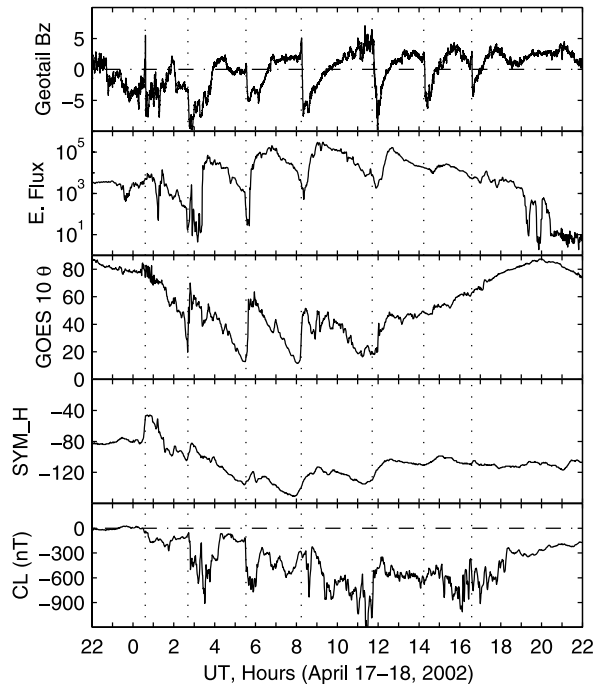

Figure 10. A comparison among the magnetic field B_z (nT) measured by Geotail, electron flux of 105–150 keV measured by LANL 1990–095, magnetic field dipolarization angle (deg) measured by GOES 10, SYM-H component (nT), and CL index between 2200 UT on 17 April and 2200 UT on 18 April 2002. The vertical dotted lines indicate the times of the southward turnings of the magnetic field B_z component measured by Geotail.

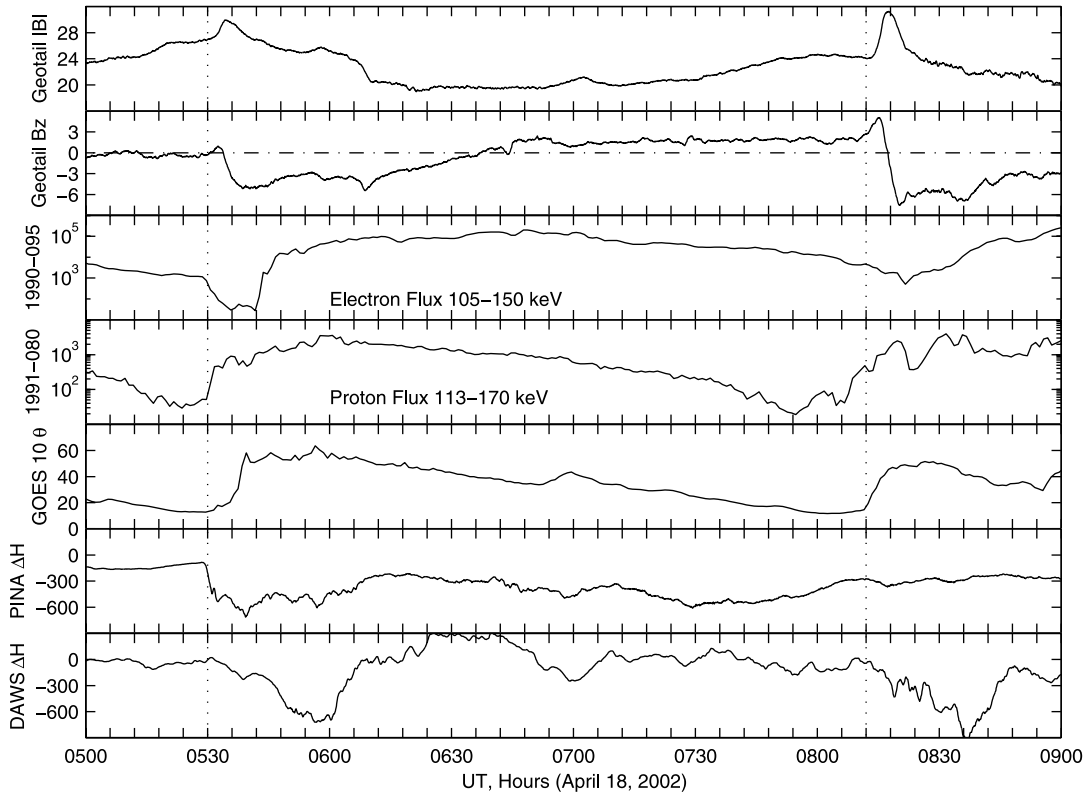

Figure 11. A detailed comparison among the magnetic field strength B (nT) and B_z (nT) component measured by Geotail, electron flux of 105–150 keV measured by LANL 1990–095, proton flux of 113–170 keV measured by LANL 1991–080, magnetic field dipolarization angle (deg) measured by GOES 10, and magnetometer deviation H component at PINA and DAWS between 0500 and 0900 UT on 18 April 2002. The vertical dotted lines at 0530 and 0812 UT indicate sudden changes in these

from the region with open field lines and therefore had much lower energy and pressure. The duration of 40–60 min in the tailward flow is consistent with the 57-min duration of persistent southward B_z during the expansion phase in the first case. The tailward velocity of 600–1000 km s^{-1} is consistent with the tailward velocity of isolated plasmoids [*Hones et al.*, 1984; *Baker et al.*, 1987; *Nagai et al.*, 1998a, 1998b; *Ieda et al.*, 1998; *Slavin et al.*, 1998]. Therefore the Geotail measurements given in Figure 15 are interpreted as periodic near-tail reconnection and plasmoid formations. Each cycle of periodic plasmoids has characteristics similar to an isolated plasmoid. The periodic reconnection onsets and plasmoids may be triggered by the solar wind pressure impulse.

[29] As shown in the first case, each reconnection onset in the near tail is related to an injection of energetic plasma particles at geosynchronous orbit. The same occurred in the second case. Figure 16 shows the electron and proton fluxes measured by the geosynchronous satellites LANL-97A and 1994–084 on 18 February 1999; the vertical dotted lines indicate the southward turnings of the Geotail magnetic field B_z (reconnection onsets) identified from Figure 15. The fluxes did not show a dropout before the increase at 0250 UT, and there was no southward turning of B_z at 0250 UT (Figure 15a). Therefore the first flux increase at 0250 UT was related to the sudden compression of the magnetosphere, rather than a substorm injection. After 0250 UT, the fluxes decreased gradually and then increased rapidly; the variations are interpreted as the flux dropouts and injections during periodic substorms, similar to the first case. There is a short-lived flux increase between 1700 and 1800 UT; it is not certain whether the temporal increase of the fluxes represents a separate substorm or a pseudobreakup.

[30] Finally, we compare different measurements of the second case. Figure 17 shows the magnetospheric magnetic field B_z component measured by Geotail in the near tail, the electron flux of 105–115 keV measured by the LANL 1994–084 satellite at geosynchronous orbit, the geomagnetic disturbance symmetric component SYM-H, and the auroral electrojet (*AE*) index. No magnetic field data are available from the GOES satellites in this case. The vertical dotted lines again indicate the southward turnings of the Geotail B_z. There is a good correspondence in different measurements. SMY-H again shows an increase and then a decrease after each injection. The *AE* index, which is widely used to represent substorm activity, always showed a large increase after each reconnection onset. The only exception is that the *AE* increase after 1600 UT lagged the corresponding injection and that the short-lived flux increase between 1700 and 1800 UT was not reflected in *AE*. We checked the CANOPUS photometer data (not shown here). The meridian scanning photometers measured very strong intensifications of the auroral emissions at ~0450 UT, and the band of the intensified auroral emissions moved toward lower latitudes before the

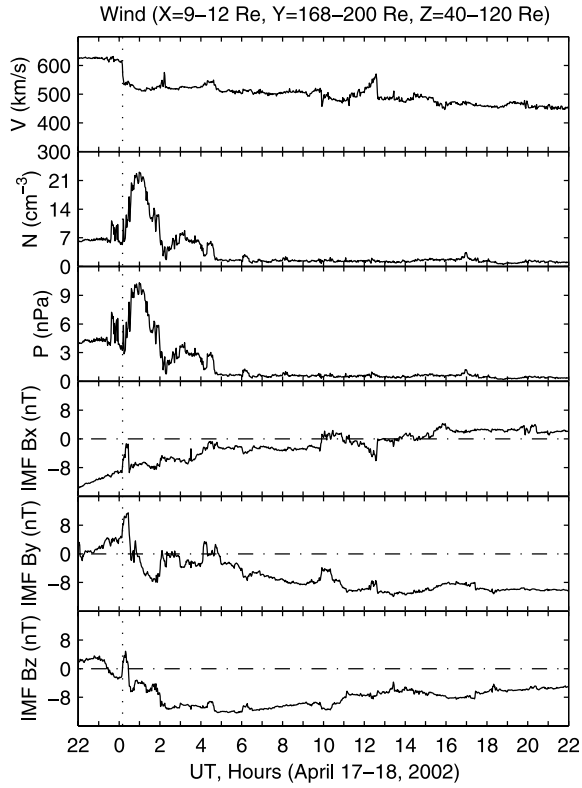

Figure 12. Solar wind velocity, solar wind ion density, solar wind dynamic pressure, and interplanetary magnetic field (IMF) components measured by the Wind spacecraft between 2200 UT on 17 April and 2200 UT on 18 April 2002. The Wind position and IMF data are given in GSM coordinates.

substorm onset at 0450 UT and then toward higher latitudes after the onset. The auroral intensifications and latitudinal motion are very similar to those in the first case. All measurements in this second case are consistent with the scenario of periodic substorms.

3. Discussion

[31] The general features of sawtooth injections at geosynchronous orbit, that is, gradual dropouts and rapid increases, have been reported by *Borovsky et al.* [1993] and *Belian et al.* [1995]. *Reeves et al.* [2003] have found that the sawtooth injections at geosynchronous orbit are associated with strong stretching and dipolarization seen in the inner magnetosphere (measured by the GOES satellites), with ENA emission enhancements seen by the IMAGE MENA/HENA instruments, with auroral substorm onsets seen by the IMAGE FUV/WIC, and with increases in SYM-H. The observations presented in our paper show that the correspondence among the sawtooth injections at geosynchronous orbit, the magnetic dipolarization in the inner magnetosphere, the auroral substorm onsets, and the increases in SYM-H is very good. These observations in our case confirm the results of *Reeves et al.* [2003].

[32] One of the major new findings, a very important aspect of the observations, reported in our paper is the establishment of the correlation of the periodic southward

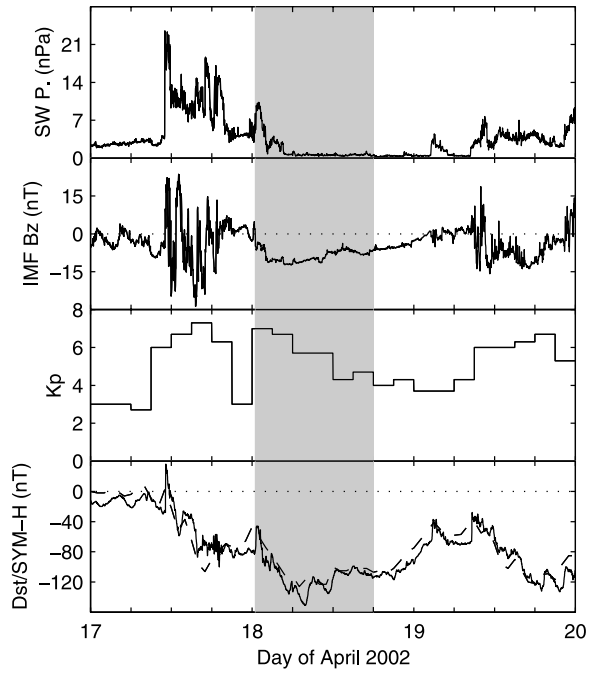

Figure 13. The solar wind dynamic pressure, IMF B_z component, *Kp* index, *Dst* index (dashed line), and SYM-H (solid line) during 17–19 April 2002. The shaded intervals indicate the occurrence of periodic substorms.

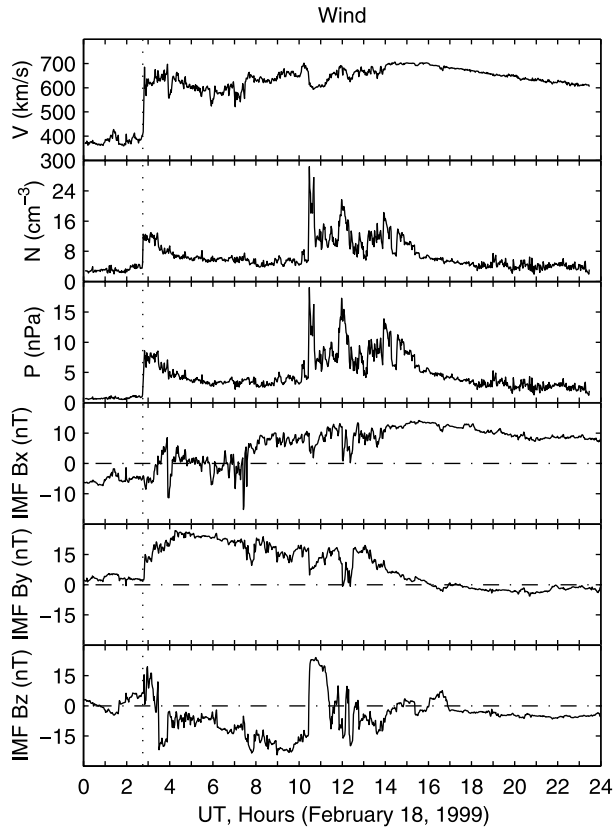

Figure 14. Solar wind velocity, solar wind ion density, solar wind dynamic pressure, and IMF components measured by the Wind spacecraft on 18 February 1999. The Wind position and IMF data are given in GSM coordinates.

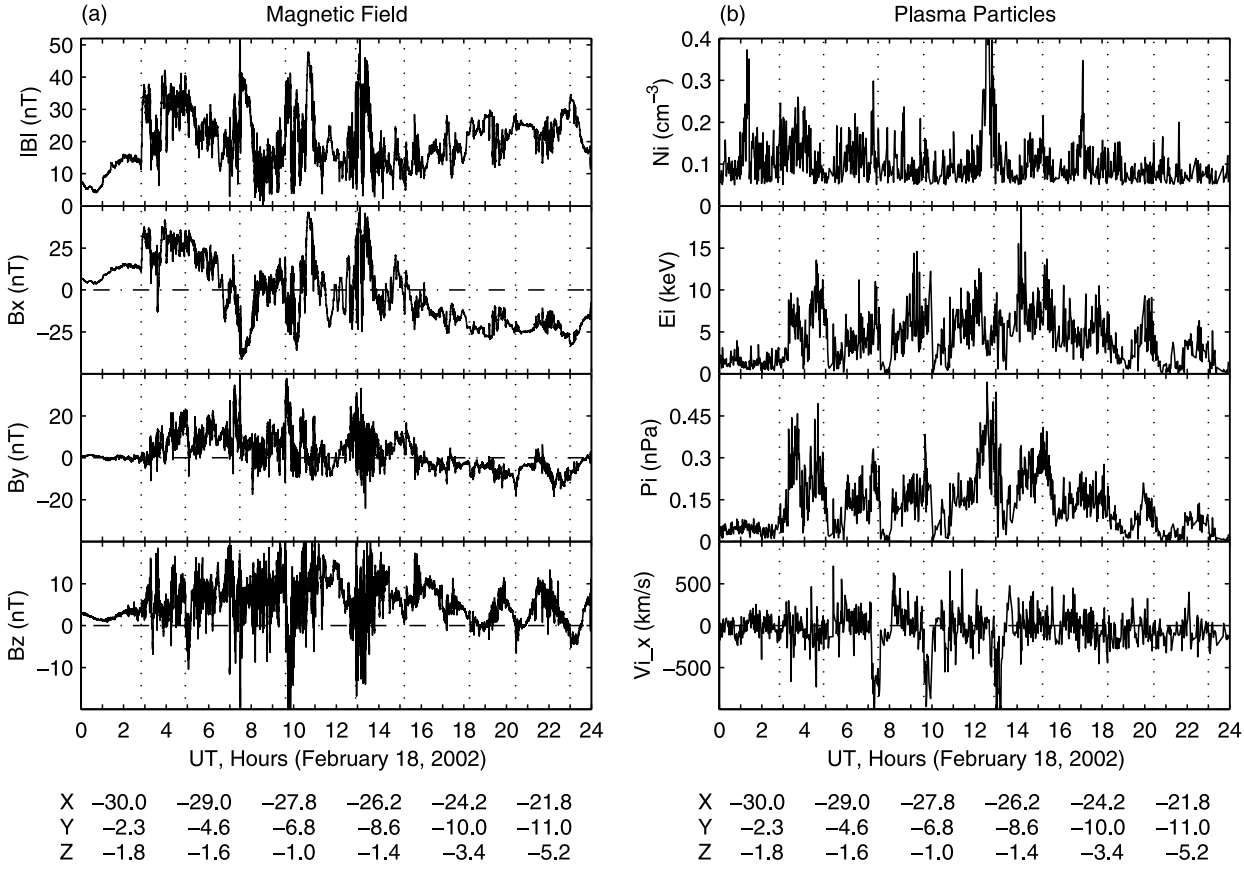

Figure 15. (a) The magnitude and components of the magnetospheric magnetic field and (b) the ion density, ion energy, ion pressure, and ion velocity measured by the Geotail spacecraft on 18 February 1999. The magnetic field components and Geotail position at the bottom of the figure are given in GSM coordinates. The vertical dotted lines indicate the southward turnings of the B_z component.

turnings of the near-tail magnetic field and geosynchronous sawtooth injections. Such southward turnings of B_z have been interpreted as the signature of near-tail reconnection onsets [*Slavin et al.*, 1984, 1993; *Taguchi et al.*, 1998; *Huang*, 2002]. Each near-tail reconnection event has a clearly associated sawtooth injection at geosynchronous orbit. The intensifications of ENA emissions in the ring current show that the flux increases indeed represent plasma particle injections from the tail to the inner magnetosphere. Another important finding is the periodic latitudinal variations of the enhanced auroral activity in association with the periodic near-tail reconnection onsets. The auroral intensifications measured by the photometers started to occur at very low magnetic latitudes ($\sim 60^\circ$) at the onsets and moved rapidly toward high latitudes during the expansion phase. The sawtooth injections are related to periodic auroral brightenings/intensifications and periodic *AE* increases. Other new results include the precise timing of the near-tail reconnection and auroral onsets, the good correspondence among all substorm signatures, the relationship of the periodic substorms with the SAPS phenomenon at subauroral latitudes, and the same periodicity in all measurements.

[33] The periodic substorms occurred after a solar wind pressure impulse impinged on the magnetosphere during the main phase and/or initial recovery phase of magnetic storms, while the solar wind did not show periodic variations. The solar wind pressure impulses may have excited the periodic substorms, while the period of the substorms is determined by the magnetosphere. *Huang et al.* [2003] suggest that magnetospheric substorms have an intrinsic cycle time of 2–3 hours. Some magnetospheric resonant state may be excited by solar wind pressure oscillations or impulses. The magnetosphere is highly dynamic during magnetic storms, which are conducive to the generation of periodic substorms. The observations in this paper are completely consistent with, and provide further support to, the conclusions of *Huang et al.* [2003].

[34] It is important to emphasize that the periodic substorms occur when the magnetosphere is continuously driven during persistent southward IMF. Each substorm does not have to be triggered by either negative or positive IMF B_z, or by a solar wind pressure impulse. This implies that the periodic substorms are related to some internal magnetospheric processes. *Lee et al.* [1985] have performed a simulation study of magnetospheric substorms. They show that under a constant driving force (corresponding to continuous southward IMF) of longer than 6 hours, the magnetic fields in the magnetotail reconnect impulsively and the formation of plasmoids occurs repeatedly every 2–4 hours. The simulations reveal that substorms can be recurrent even if the solar wind driver is stable. They suggest that the impulsive reconnections are associated with the internal

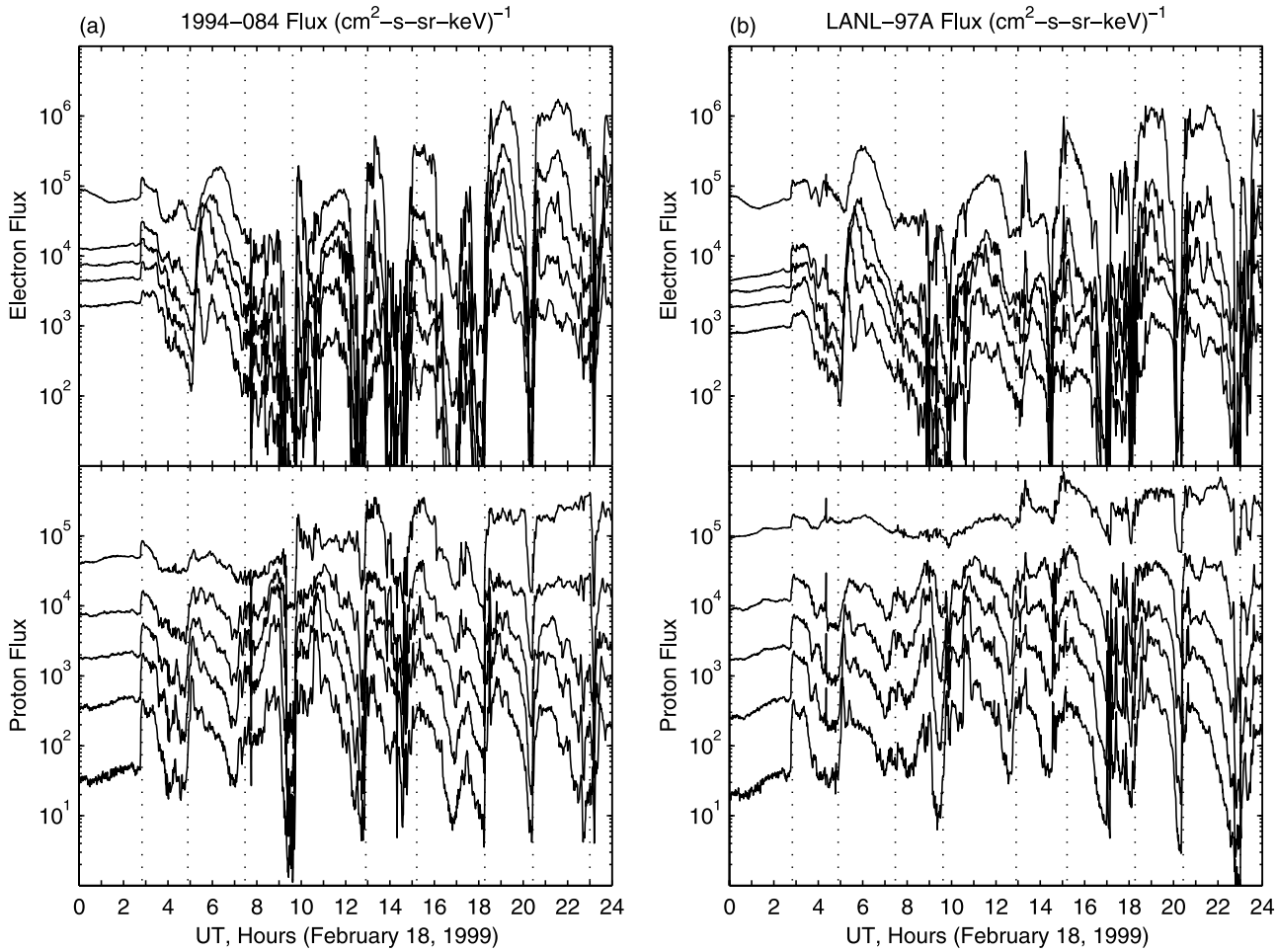

Figure 16. Electron and proton fluxes measured by the geosynchronous satellites 1994–084 and LANL-97A on 18 February 1999. The vertical dotted lines indicate the times of the southward turnings of the B_z component measured by Geotail, identified from Figure 15.

dynamics and instability of the magnetotail. A number of magnetospheric instabilities have been suggested to be potential internal triggers of substorms [*Lui*, 1996, and references therein; *Heikkila et al.*, 2001]. In the case of 18 April 2002 presented in our paper, the IMF was continuously southward for 24 hours, and the magnetospheric magnetic field in the near tail turned southward periodically, with a mean period of 2.7 hours. As discussed in the previous section, such a magnetic signature has been interpreted as periodic reconnection onsets and plasmoid formations [*Slavin et al.*, 1984, 1993; *Taguchi et al.*, 1998; *Huang*, 2002]. The observations and interpretation in our paper are consistent with the simulation results of *Lee et al.* [1985].

[35] The Geotail satellite was in an ideal location for monitoring the reconnection onsets in the two cases reported in this paper. Here we take the first case of 18 April 2002 as an example. Geotail detected periodic reconnection onsets and plasmoid formations when the satellite was located between $X_{GSM} = -22$ and -28 R_E. Associated with each reconnection onset, there was an increase in the magnetic field strength and in the B_z component before B_z became negative; the details of this phenomenon have been analyzed by *Huang* [2002]. The increase in $|B|$ and B_z implies that the satellite was located tailward of the plasmoid center when the plasmoid was forming and the distance between the reconnection site and Geotail must be larger than half of the plasmoid length. *Moldwin and Hughes* [1992] found that the average length of plasmoids is 16 ± 13 R_E, and *Slavin et al.* [1993, 1998] derived plasmoid lengths of 27–40 R_E. *Ieda et al.* [1998] showed that the average length of plasmoids depends on the downtail distance, varying from $\sim$4 R_E in the near tail to $\sim$10 R_E in the distant tail. In our case, Geotail detected the plasmoids when it was located at $X_{GSM} = -24$ R_E. Even though we assume that the length of the plasmoids in our case was 4–10 R_E, the corresponding magnetic reconnection must occur between $X_{GSM} = -19$ and -22 R_E. *Nagai et al.* [1998b] made a statistical study of the near-tail reconnection region and found that the reconnection occurs between $X_{GSM} = -20$ and -30 R_E. The inferred reconnection site in our case is near the earthward end of the reconnection region derived by *Nagai et al.* [1998b].

[36] Magnetic reconnection in a near-Earth neutral line is a widely accepted mechanism responsible for the generation of isolated substorms [*Hones et al.*, 1984; *Baker et al.*, 1987, 1996; *Nagai et al.*, 1998a, 1998b; *Ieda et al.*, 1998; *Slavin et al.*, 1998]. In this paper, we have shown that reconnection onsets can be periodic in the near tail. We have

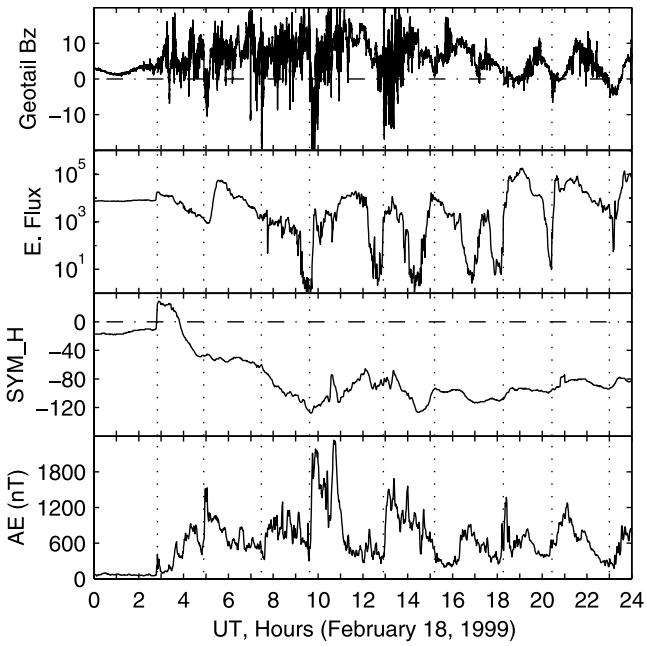

Figure 17. A comparison among the magnetic field B_z (nT) measured by Geotail, electron flux of 105–150 keV measured by LANL 1994–084, SYM-H component (nT), and *AE* index (nT) on 18 February 1999.

also shown that periodic reconnection onsets are well correlated with other typical substorm signatures. Therefore the near-tail reconnection is identified as the mechanism responsible for the periodic substorms. The periodic reconnection onsets cause periodic injections of energetic plasma particles at geosynchronous orbit, and the sawtooth injections indeed represent periodic substorm onsets. Each cycle of the periodic substorms has the characteristics similar to those of an isolated substorm. The characteristics include the near-tail reconnection, the energetic plasma particle injection at geosynchronous orbit, the magnetic field dipolarization in the inner magnetosphere, the variation in the ring current, the auroral brightening and intensification, the equatorward motion of the auroral emission band during the growth phase and poleward motion during the expansion phase, and the increase in the *AE* index.

[37] Figures 6 and 8 show that the auroral emission band moved equatorward during the growth phase of substorms and the onset occurred at low latitudes ($\sim$61° magnetic latitude near midnight). Such a low latitude and corresponding L shell (4.25) appear to be far from the reconnection onset in the tail ($X_{GSM} = -20\ R_E$ or further tailward). Similar equatorward motion of the auroral emission band during the growth phase of an isolated substorm and subsequent poleward motion during the expansion phase were reported by *Samson et al.* [1992]. They suggested that the region of intense electron and proton precipitation, which causes the auroral intensification, is equatorward of the nightside magnetospheric open-closed field line boundary. The equatorward motion of the particle precipitation is due to an increasing cross-tail current near the Earth during the growth phase of substorms, indicating that some component of the substorm mechanism must be active very close to the Earth.

[38] The current disruption, which occurs in the near-Earth magnetosphere, is another candidate of the mechanisms responsible for the generation of substorms [*Lui*, 1991, 1996]. In the current disruption scenario, the substorm onset location is near the boundary between the tail-like and the dipolar-like field regions, the disruption arises from some plasma instabilities, and the antisunward expansion of the current reduction in the tail may correspond to the poleward motion of the active aurora in the ionosphere during the substorm expansion phase. Launching of rarefaction waves downstream may lead to plasma sheet thinning and subsequent formation of large-scale X line in the tail ($X_{GSM} = -20\ R_E$ or further tailward). A key point in the current disruption scenario is that the onset location is in the near-Earth region between $X_{GSM} = -6$ and $-10\ R_E$ and that the rarefaction waves launched in the disruption region lead to the X-line reconnection in the tail. In the near-Earth neutral line model of substorms [*Hones*, 1984; *Baker et al.*, 1996], magnetic reconnection occurs first in the midtail, and earthward plasma flow from the neutral line carries northward magnetic flux, which thickens the plasma sheet in the inner magnetotail as flux accumulates [*Birn and Hesse*, 1996]. The reconnection sends a flow burst earthward, and the auroral breakup and field dipolarization start when the flow is slowed and diverted in the inner magnetosphere. In our observations, the auroral onsets occurred at low latitudes and then moved toward higher latitudes during the expansion phase, which appears to be consistent with the current disruption scenario. However, no time delay can be identified between the auroral onset and near-tail reconnection in our case, and it is not clear whether the current disruption or the near-tail reconnection occurs first. What is definite in our case is that periodic near-tail reconnection onsets occur and that the periodic reconnection is associated with sawtooth injections at geosynchronous orbit.

4. Conclusions

[39] We have presented and analyzed the multiple instrumental measurements of periodic magnetospheric substorms from solar wind triggering to southward turnings of the near-tail magnetospheric magnetic field to processes at geosynchronous orbit and in the inner magnetosphere and to auroral activity during the April 2002 and February 1999 magnetic storms. The major findings of this study are as follows:

[40] 1. Periodic variations in the magnetospheric magnetic field and plasma parameters occurred in the near tail and were measured by the Geotail satellite which was located between $X_{GSM} = -21$ and $-30\ R_E$. As many as seven cycles of the variations were detected in each case, with a mean period of $\sim$2.7 hours. For each cycle of the variation, the strength of the magnetic field was increased, the B_z component of the geomagnetic field turned southward, and the plasma flow became tailward with a speed of 600–1000 km s^{-1}. The magnetospheric variations are identified as periodic reconnection onsets in a near-Earth neutral line and subsequent plasmoid formations in association with periodic substorms.

[41] 2. Periodic variations of energetic plasma particle fluxes were measured by geosynchronous satellites. The flux variations exhibit a well-defined sawtooth shape, with gradual flux decreases followed by rapid flux increases. The flux

dropouts occurred during the growth phase of substorms, and the flux increases occurred after the substorm onsets. Associated with each flux increase is an enhancement of the emissions of energetic neutral atoms in the ring current, indicating that new plasma particles were injected into the ring current. This verifies that the increases of the plasma particle fluxes at geosynchronous orbit represent true injections from the tail to the inner magnetosphere and that the injections can be used to represent substorm onsets. Another process in the inner magnetosphere associated with the flux injections is the periodic dipolarization of the magnetic field.

[42] 3. The signature of periodic auroral substorms and auroral brightenings and intensifications was measured by the IMAGE satellite and by the Canadian CANOPUS photometers. Periodic enhancements in the auroral electrojet current, as well as in the CL and *AE* indices, were measured by ground magnetometers. For each cycle of the auroral substorms, a band of enhanced auroral emissions moved equatorward during the growth phase and poleward after the onset. The periodic auroral substorms correlated well with the periodic reconnection onsets in the near tail.

[43] 4. The observations show that magnetospheric substorms can be indeed periodic during magnetic storms. The mean period of the substorms in the cases studied is $\sim$2.7 hours. The periodic substorms occur when the magnetosphere is continuously driven under continuous southward IMF and stable solar wind pressure conditions, and each substorm does not have to be triggered by either a northward IMF turning or a solar wind pressure impulse. The generation of the periodic substorms is related to periodic magnetic reconnection in a near-Earth neutral line. Each cycle of the periodic substorms includes the following processes: a reconnection onset in the near tail, an injection of energetic plasma particles at geosynchronous orbit, an enhancement of energetic neutral atom emissions in the ring current, a magnetic dipolarization in the inner magnetosphere, an intensification and brightening in the auroral emissions, a latitudinal motion of the enhanced auroral emission band, and an increase of the *AE* index. There is an excellent correspondence among the magnetospheric and ionospheric substorm signatures; all the substorm signatures have the same periodicity.

[44] **Acknowledgments.** Work at MIT Haystack Observatory was supported by a NSF cooperative agreement with Massachusetts Institute of Technology. We thank Fokke Creutzberg for producing the auroral luminosity plot of the CANOPUS meridian scanning photometers and the Canadian Space Agency for providing the ground magnetoemeter data. The Geotail data are provided by S. Kokubun through DARTS at the Institute of Space and Astronautical Science (ISAS) in Japan. The IMAGE MENA data are provided by Southwest Research Institute and the IMAGE FUV/WIC data are provided by Space Sciences Laboratory, University of California, Berkeley. The SYM-H data are provided by the World Data Center for Geomagnetism at Kyoto University. We acknowledge the CDAWeb for access to the Wind, GOES 8, and GOES 10 data.

[45] Lou-Chuang Lee thanks the two reviewers for their assistance in evaluating this paper.

References

Akasofu, S. I., *Polar and Magnetospheric Substorms*, D. Reidel, Norwell, Mass., 1968.

Baker, D. N., R. C. Anderson, R. D. Zwickl, and J. A. Slavin, Average plasma and magnetic field variations in the distant magnetotail associated with near-Earth substorm effects, *J. Geophys. Res.*, *92*, 71, 1987.

Baker, D. N., T. I. Pulkkinen, V. Angelopoulos, W. Baumjohann, and R. L. McPherron, Neutral line model of substorms: Past results and present view, *J. Geophys. Res.*, *101*, 12,975, 1996.

Baumjohann, W., M. Hesse, S. Kokubun, T. Mukai, T. Nagai, and A. A. Petrukovich, Substorm dipolarization and recovery, *J. Geophys. Res.*, *104*, 24,995, 1999.

Belian, R. D., T. E. Cayton, and G. D. Reeves, Quasi-periodic global substorm generated flux variations observed at geosynchronous orbit, in *Space Plasmas*: *Coupling Between Small and Medium Scale Processes*, *Geophys. Monogr. Ser.*, vol. 89, edited by M. Ashour-Abdalla, T. Chang, and P. Dusenbery, pp. 143–148, AGU, Washington, D. C., 1995.

Birn, J., and M. Hesse, Details of current disruption and diversion in simulations of magnetotail dynamics, *J. Geophys. Res.*, *101*, 15,345, 1996.

Borovsky, J. E., R. J. Nemzek, and R. D. Belian, The occurrence rate of magnetospheric substorm onsets: Random and periodic substorms, *J. Geophys. Res.*, *98*, 3807, 1993.

Burch, J. L., et al., Views of Earth's magnetosphere with the IMAGE satellite, *Science*, *291*, 629, 2001.

Fairfield, D. H., et al., Geotail observations of substorm onset in the inner magnetotail, *J. Geophys. Res.*, *103*, 103, 1998.

Foster, J. C., and W. J. Burke, SAPS: A new categorization for sub-auroral electric fields, *EOS Trans. AGU*, *83*, 393, 2002.

Foster, J. C., and H. B. Vo, Average characteristics and activity dependence of the subauroral polarization stream, *J. Geophys. Res.*, *107*(A12), 1475, doi:10.1029/2002JA009409, 2002.

Heikkila, W., T. Chen, Z. X. Liu, Z. Y. Pu, R. J. Pellinen, and T. I. Pulkkinen, Near Earth current meander (NECM) model of substorms, *Space Sci. Rev.*, *95*, 399, 2001.

Hones, E. W., Jr., Plasma sheet behavior during substorms, in *Magnetic Reconnection in Space and Laboratory Plasmas*, *Geophys. Monogr. Ser.*, vol. 30, edited by E. W. Hones Jr., pp. 178–184, AGU, Washington, D. C., 1984.

Hones, E. W., Jr., D. N. Baker, S. J. Bame, W. C. Feldman, J. T. Gosling, D. J. McComas, R. D. Zwickl, J. A. Slavin, E. J. Smith, and B. T. Tsurutani, Structure of the magnetotail at 200 R_E and its response to geomagnetic activity, *Geophys. Res. Lett.*, *11*, 5, 1984.

Huang, C. S., Evidence of periodic (2–3 hour) near-tail magnetic reconnection and plasmoid formation: Geotail observations, *Geophys. Res. Lett.*, *29*(24), 2189, doi:10.1029/2002GL016162, 2002.

Huang, C. S., J. C. Foster, and J. M. Holt, Westward plasma drift in the midlatitude ionospheric *F* region in the midnight-dawn sector, *J. Geophys. Res.*, *106*, 30,349, 2001.

Huang, C. S., G. D. Reeves, J. E. Borovsky, R. M. Skoug, Z. Y. Pu, and G. Le, Periodic magnetospheric substorms and their relationship with solar wind variations, *J. Geophys. Res.*, *108*(A6), 1255, doi:10.1029/2002JA009704, 2003.

Ieda, A., S. Machida, T. Mukai, Y. Saito, T. Yamamoto, A. Nishida, T. Terasawa, and S. Kokubun, Statistical analysis of the plasmoid evolution with Geotail observations, *J. Geophys. Res.*, *103*, 4453, 1998.

Iyemori, T., and D. R. K. Rao, Decay of the *Dst* field of geomagnetic disturbance after substorm onset and its implication to storm-substorm relation, *Ann. Geophys.*, *14*, 608, 1996.

Lee, L. C., Z. F. Fu, and S. I. Akasofu, A simulation study of forced reconnection processes and magnetospheric storms and substorms, *J. Geophys. Res.*, *90*, 10,896, 1985.

Lui, A. T. Y., A synthesis of magnetospheric substorm models, *J. Geophys. Res.*, *96*, 1849, 1991.

Lui, A. T. Y., Current disruption in the Earth's magnetosphere: Observations and models, *J. Geophys. Res.*, *101*, 13,067, 1996.

McPherron, R. L., C. T. Russell, and M. P. Aubry, Satellite studies of magnetospheric substorms on August 15, 1968: 9. Phenomenological model for substorms, *J. Geophys. Res.*, *78*, 3131, 1973.

Moldwin, M. B., and W. J. Hughes, On the formation and evolution of plasmoids: A survey of ISEE 3 geotail data, *J. Geophys. Res.*, *97*, 19,259, 1992.

Moldwin, M. B., M. F. Thomsen, S. J. Bame, D. J. McComas, J. Birn, G. D. Reeves, R. Nemzek, and R. D. Belian, Flux dropouts of plasma and energetic particles at geosynchronous orbit during large geomagnetic stroms: Entry into the lobes, *J. Geophys. Res.*, *100*, 8031, 1995.

Nagai, T., M. Fujimoto, M. S. Nakamura, R. Nakanura, Y. Saito, T. Mukai, T. Yamamoto, A. Nishida, and S. Kokubun, A large southward magnetic field of -23.5 nT in the January 10, 1995, plasmoid, *J. Geophys. Res.*, *103*, 4441, 1998a.

Nagai, T., M. Fujimoto, Y. Saito, S. Machida, T. Terasawa, R. Nakamura, T. Yamamoto, T. Mukai, A. Nishida, and S. Kokubun, Structure and dynamics of magnetic reconnection for substorm onsets with Geotail observations, *J. Geophys. Res.*, *103*, 4419, 1998b.

Ohtani, S., S. Kokubun, and C. T. Russell, Radial expansion of the tail current disruption during substorms: A new approach to the substorm onset region, *J. Geophys. Res.*, *97*, 3129, 1992.

Pu, Z. Y., et al., Ballooning instability in the presence of a plasma flow: A synthesis of tail reconnection and current disruption models for the initiation of substorms, *J. Geophys. Res.*, *104*, 10,235, 1999.

Reeves, G. D., and M. G. Henderson, The storm-substorm relationship: Ion injections in geosynchronous measurements and composite energetic neutral atom images, *J. Geophys. Res.*, *106*, 5833, 2001.

Reeves, G. D., T. A. Fritz, T. E. Cayton, and R. D. Belian, Multi-satellite measurements of the substorm injection region, *Geophys. Res. Lett.*, *17*, 2015, 1990.

Reeves, G. D., G. Kettmann, T. A. Fritz, and R. D. Belian, Further investigation of the CDAW 7 substorm using geosynchronous particle data: Multiple injections and their implications, *J. Geophys. Res.*, *97*, 6417, 1992.

Reeves, G. D., et al., IMAGE, POLAR, and geosynchronous observations of substorm and ring current ion injection, in *Storm-Substorm Relationship*, *Geophys. Monogr. Ser.*, AGU, Washington, D. C., in press, 2003.

Rostoker, G., J. C. Samson, F. Creutzberg, T. J. Hughes, D. R. McDiarmid, A. G. McNamara, A. V. Jones, D. D. Wallis, and L. L. Cogger, CANOPUS—A ground based instrument array for remote sensing the high latitude ionosphere during the ISTP/GGS program, *Space Sci. Rev.*, *71*, 743, 1995.

Roux, A., S. Perraut, P. Robert, A. Morane, A. Pedersen, A. Korth, G. Kremser, B. Aparicio, D. Rodgers, and R. Pellinen, Plasma sheet instability related to the westward traveling surge, *J. Geophys. Res.*, *96*, 17,697, 1991.

Samson, J. C., L. R. Lyons, P. T. Newell, F. Creutzberg, and B. Xu, Proton aurora and substorm intensifications, *Geophys. Res. Lett.*, *19*, 2167, 1992.

Siscoe, G. L., and H. E. Petschek, On storm weakening during substorm expansion phase, *Ann. Geophys.*, *15*, 211, 1997.

Slavin, J. A., E. J. Smith, B. T. Tsurutani, D. G. Sibeck, H. J. Singer, D. N. Baker, J. T. Gosling, E. W. Hones, and F. L. Scarf, Substorm associated traveling compression regions in the distant tail: ISEE-3 geotail observations, *Geophys. Res. Lett.*, *11*, 657, 1984.

Slavin, J. A., M. F. Smith, E. L. Mazur, D. N. Baker, E. W. Hones Jr., T. Iyemori, and E. W. Greenstadt, ISEE 3 observations of traveling compression regions in the Earth's magnetotail, *J. Geophys. Res.*, *98*, 15,425, 1993.

Slavin, J. A., et al., ISTP observations of plasmoid ejections: IMP 8 and Geotail, *J. Geophys. Res.*, *103*, 119, 1998.

Taguchi, S., J. A. Slavin, and R. P. Lepping, Traveling compression regions in the midtail: Fifteen years of IMP 8 observations, *J. Geophys. Res.*, *103*, 17,641, 1998.

Thomsen, M. F., S. J. Bame, D. J. McComas, M. B. Moldwin, and K. R. Moore, The magnetospheric lobe at geosynchronous orbit, *J. Geophys. Res.*, *99*, 17,283, 1994.

Yeh, H. C., J. C. Foster, F. J. Rich, and W. Swider, Storm time electric field penetration observed at midlatitude, *J. Geophys. Res.*, *96*, 5707, 1991.

J. C. Foster and C.-S. Huang, Haystack Observatory, Massachusetts Institute of Technology, Route 40, Westford, MA 01886, USA. (jcf@haystack.mit.edu; cshuang@haystack.mit.edu)

H. U. Frey, Space Science Laboratory, University of California, Centennial Drive at Grizzly, Peak Blvd, Berkeley, CA 94720, USA. (hfrey@ssl.berkeley.edu)

J.-M. Jahn and C. J. Pollock, Department of Space Science, Southwest Research Institute, San Antonio, TX 78228, USA. (jjahn@swri.edu; cpollock@swri.edu)

G. Le, Electrodynamics Branch, Laboratory for Extraterrestrial Physics, NASA Goddard Space Flight Center, Greenbelt, MD 20771, USA. (guan.le@gsfc.nasa.gov)

G. D. Reeves, Los Alamos National Laboratory, Mail Stop D-466, Los Alamos, NM 87545, USA. (reeves@lanl.gov)